nature neuroscience

Reactivations of emotional memory in the hippocampus–amygdala system during sleep

Gabrielle Girardeau[1], Ingrid Inema[1,4] & György Buzsáki[1–3]

The consolidation of context-dependent emotional memory requires communication between the hippocampus and the basolateral amygdala (BLA), but the mechanisms of this process are unknown. We recorded neuronal ensembles in the hippocampus and BLA while rats learned the location of an aversive air puff on a linear track, as well as during sleep before and after training. We found coordinated reactivations between the hippocampus and the BLA during non-REM sleep following training. These reactivations peaked during hippocampal sharp wave–ripples (SPW-Rs) and involved a subgroup of BLA cells positively modulated during hippocampal SPW-Rs. Notably, reactivation was stronger for the hippocampus–BLA correlation patterns representing the run direction that involved the air puff than for the 'safe' direction. These findings suggest that consolidation of contextual emotional memory occurs during ripple-reactivation of hippocampus–amygdala circuits.

Cooperation between amygdala, particularly the BLA, and hippocampus is critical for contextual emotional memory[1–10]. It is believed that the emotional and spatial components of an experience are processed by the amygdala and dorsal hippocampal circuits, respectively[8,11–13]. Lesion and other experiments have shown that fine spatial representation in the dorsal hippocampus[14,15] is required for spatial and contextual memory, including context–threat associations, with a limited contribution from the ventral hippocampus[11,16–21]. Because only the ventral hippocampus and associated entorhinal outputs project directly to the amygdala, including the BLA and central amygdala[10,22,23], it remains to be determined how emotional and contextual stimuli are combined and consolidated to form a stable, integrated representation of the context and associated emotional valence.

Sleep replay of wake sequences of place cells during hippocampal SPW-Rs are instrumental for spatial memory consolidation and the stabilization of newly formed spatial representations[24–26]. By comparison, the consolidation mechanisms of amygdala-dependent memories have only been partially explored[1,27,28]. We hypothesized that contextual emotional experience is replayed in the interconnected hippocampus–amygdala circuit during sleep. More specifically, because synchronous discharges of neuron populations during SPW-Rs facilitate the combination of neuronal information throughout the entire dorso-ventral axis of the hippocampus[29], we hypothesized that spatial information from the dorsal hippocampus may be associated with the threat representation in the BLA during SPW-Rs of non-REM (NREM) sleep.

To study hippocampus–amygdala interactions, we combined a classical spatial task with a location-specific aversive element (air puff). We recorded large neuronal ensembles simultaneously in the amygdala and dorsal hippocampus during training and sleep episodes before and after training. To identify the subpopulations of neurons in the amygdala that are functionally linked to the dorsal hippocampus, we examined their discharge patterns during SPW-Rs. We then investigated whether joint hippocampus–BLA representations of space and threat are reactivated during SPW-Rs of NREM sleep.

RESULTS

Rats learn the daily location of an aversive air puff on a linear track

To study hippocampal–amygdala reactivations, we designed a task by combining a classical spatial task with an aversive component to recruit BLA neurons. Rats (n = 4) were pretrained to run back and forth on a linear track for water rewards. After steady performance was achieved, we introduced an aversive air puff at the same location of the track on each lap in one of the running directions. The location and direction of the air puff was changed daily in a pseudo-random manner. Previous work has shown that air-puff-induced contextual fear learning relies on both the amygdala and the hippocampus[30]. We adapted this task to allow daily behavioral training and recordings of large neuronal ensembles in freely moving animals. Each daily recording session consisted of a pre-run behavioral test session on the track without the air puff, followed by pre-learning sleep in the home cage ('pre-sleep', categorized as pre-REM or pre-NREM), a training session ('run') with the air puff, post-learning sleep ('post-sleep', categorized as post-REM or post-NREM) and a post-run test session without the air puff (**Fig. 1a**). Because rats slow down before crossing the air puff location if they remember its location, we quantified memory performance from the pre-run and post-run test epochs by comparing the running speed of the rat in the danger zone of the current day (defined as the 20 cm preceding the air puff location) with the speed at the previous day's danger zone (**Fig. 1a**,**b** and **Supplementary Fig. 1a**). The current danger zone, initially neutral during pre-run, acquires an aversive valence during training, while the previous danger zone loses its aversive nature. Therefore, the systematic reversal in the speed ratio (previous/current danger zone) between pre- and

[1]New York University Neuroscience Institute, New York University, New York, New York, USA. [2]Department of Neurology, Medical Center, New York University, New York, New York, USA. [3]Center for Neural Science, New York University, New York, New York, USA. [4]Present address: Douglas Institute, McGill University, Montreal, Quebec, Canada. Correspondence should be addressed to G.B. (gyorgy.buzsaki@nyumc.org).

Received 21 February; accepted 2 August; published online 11 September 2017; doi:10.1038/nn.4637

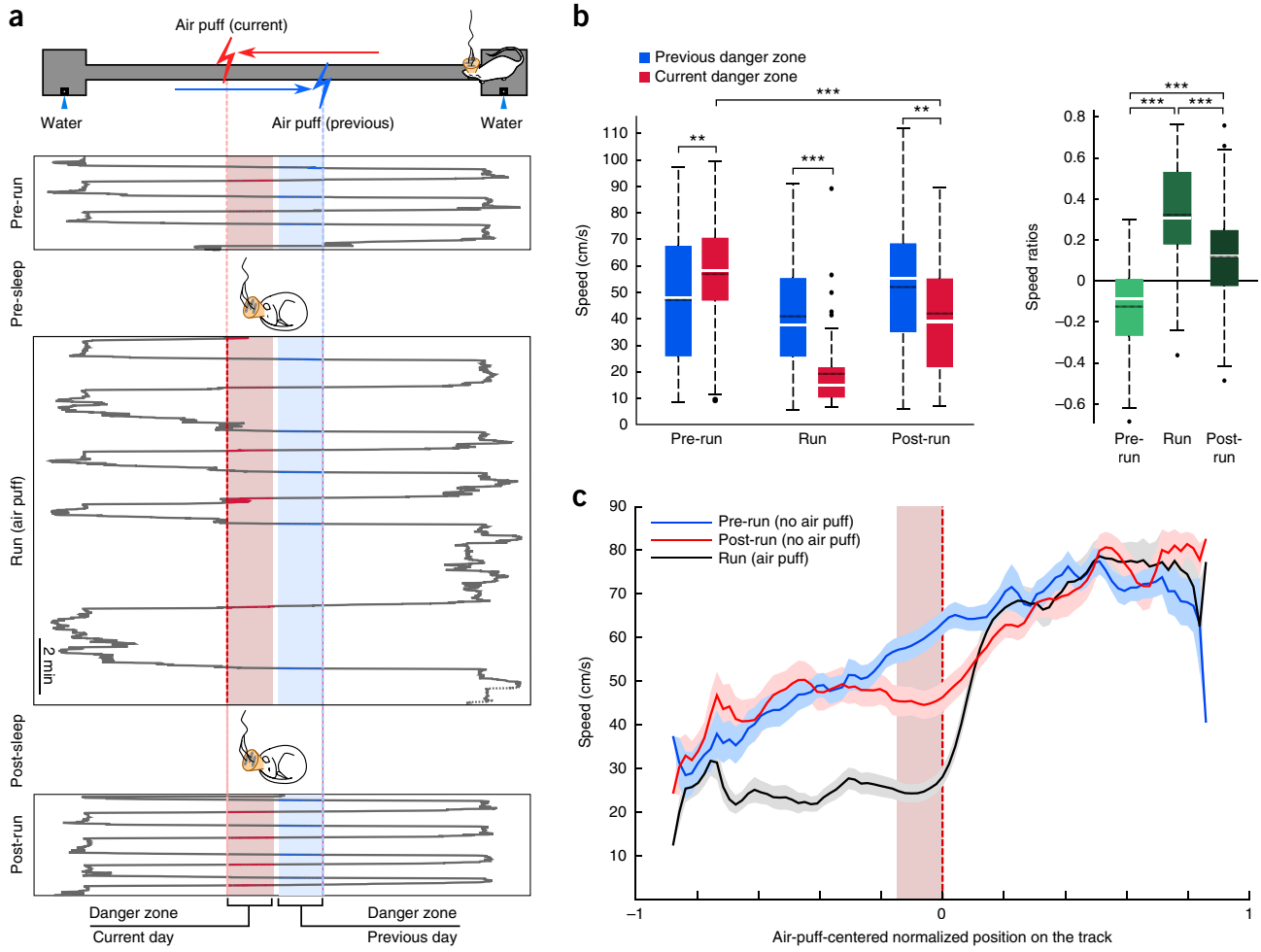

Figure 1 Rats learn the daily location of an aversive air puff. (**a**) Rats run back and forth on a linear track for water rewards. Gray line: one-dimensional position of the animal on the track over time in a representative session (one session in one animal out of 55 sessions in 4 animals). An air puff is delivered at the same location on the track in one running direction during the run epoch. The air puff location is changed every day. The run epoch is flanked by two sleep epochs (pre-sleep, post-sleep) and two test run sessions where no air puff is delivered (pre-run, post-run). The danger zones (DZ) are defined as the 20 cm preceding the location of the air puff on the current day (pink) and on the previous day (blue). (**b**) Left: speed in the current and previous DZ across animals and sessions during the three run epochs (two-way repeated measures ANOVA; $n = 55$ sessions in 4 animals; significant session effect (pre-run, run or post-run, $P = 7.48 \times 10^{-14}$, d.f. = 2, $F = 41.51$), air puff location effect (current vs. previous, $P = 0.0012$, d.f. = 1, $F = 11.81$) and interaction, ($P = 4.46 \times 10^{-11}$, d.f. = 2, $F = 30.53$). *Post hoc* paired *t*-tests showed significant differences between previous and current DZ speed for pre-run, run and post-run ($P = 0.0011$, $t(52) = 3.45$; $P = 9.70 \times 10^{-9}$, $t(51) = -6.84$; $P = 0.00307$, $t(51) = -3.10$), as well as for the current DZ between pre-run and post-run ($P = 1.21 \times 10^{-6}$, $t(53) = 5.47$). Right: speed ratios across sessions and animals (one-way repeated measure ANOVA; significant session effect, $P = 1.31 \times 10^{-13}$, d.f. = 2, $F = 40.48$; *post hoc* *t*-tests, pre-run vs. run: $P = 2.5 \times 10^{-11}$, $t(51) = -8.49$; pre-run vs. post-run $P = 5.3 \times 10^{-6}$, $t(51) = -5.08$; run vs. post-run $P = 5.1 \times 10^{-5}$, $t(50) = 4.43$; white line, median; black line, mean; black dots, outliers; boxes, first and last quartiles; whiskers, minimum and maximum values excluding outliers). $^{**}P < 0.01$, $^{***}P < 0.001$ with Bonferroni correction. (**c**) Air-puff-centered mean speed (± s.e.m., pre-run: $n = 52$ sessions in 4 animals; run and post-run: $n = 53$ sessions in 4 animals) curves in the air puff direction in the pre-test (no air puff), training and post-test (no air puff) epochs. The current DZ is indicated by the shaded pink bar. Note the slower speed in the DZ post-run compared to pre-run.

post-run indicates learning of the new air puff location (**Fig. 1b** and **Supplementary Fig. 1b**). The typical behavioral pattern on the track during run was a reduced speed before the air puff, followed by an acceleration after passing through the danger zone. A similar speed change was maintained during post-run, whereas speed smoothly increased throughout the track during pre-run (**Fig. 1c**). This was quantitatively reflected by the significantly slower speed in the current danger zone in post-run compared to pre-run (**Fig. 1b**,**c**). The aversive valence of the air puff gradually diminished with training days (**Supplementary Fig. 1c**). The location of the air puff on the track did not correlate with the speed in the current danger zone in pre-run, training or post-run, ruling out a systematic bias of the air puff location on the results.

BLA recordings and sleep physiology

We recorded ensembles of neurons from both left and right amygdala and the dorsal CA1 hippocampal region during the task (**Fig. 2a**,**b**). Eight-shank silicon probes were moved downward by 140-µm steps between each behavioral experiment. This allowed recording from large areas of the amygdala and the piriform cortex in each rat (**Supplementary Fig. 2**). Over the course of a total of 61 sessions, we recorded 7,390 well-isolated units (rat 1, 2,444; rat 2, 1,294; rat

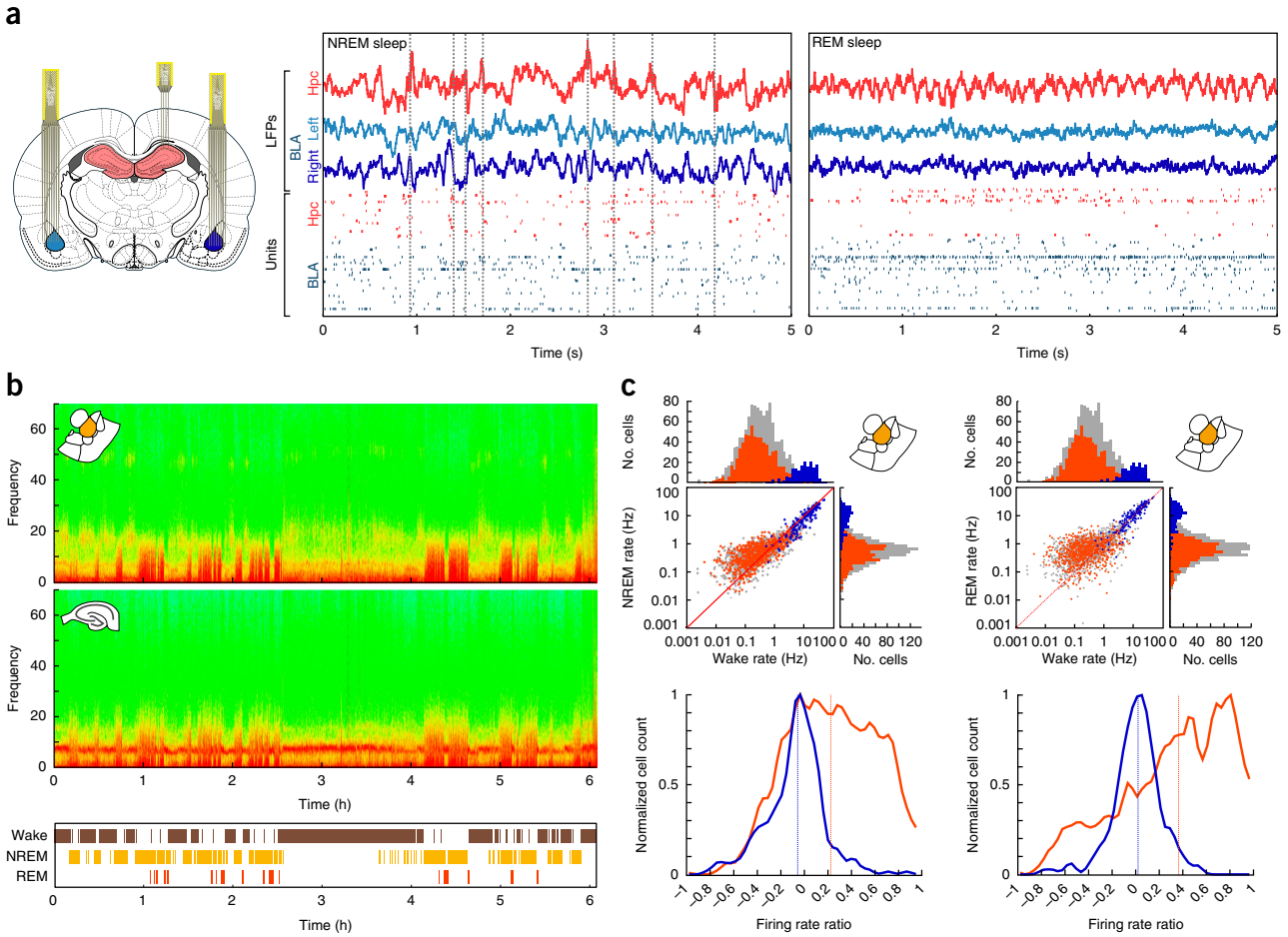

Figure 2 Physiological characterization of BLA. (**a**) Silicon probe recordings from the dorsal hippocampal CA1 (four-shank probe) and bilateral amygdala (eight-shank probes; total 160 channels) and example local field potentials (LFPs) and units (raster plots) in the hippocampus (Hpc; red) and left and right amygdala (BLA; blue). Hippocampal SPW-R times are indicated by gray lines in NREM sleep. (**b**) CA1 and BLA spectrograms for an example session (out of 29 sessions in 3 rats with simultaneous BLA and hippocampus recordings). Spectrograms were used to define brain states (wake, NREM or REM sleep; colors represent power in arbitrary units, from green (low) to red (high)). (**c**) Distributions of firing rates for monosynaptically identified pyramidal cells (orange, $n = 675$ cells; see Online Methods and **Supplementary Fig. 3**), interneurons (blue, $n = 175$ cells) and other cells (gray, $n = 1{,}188$ cells) in BLA during NREM vs. wake (top left) and REM vs. wake (top right). The distribution of REM/wake and NREM/wake firing rate ratios (bottom) is skewed toward 1 for pyramidal cells (orange, monosynaptically identified pyramidal cells; $n = 675$; NREM/wake: $P = 4.07 \times 10^{-46}$, $z = 14.25$; REM/wake: $P = 8 \times 10^{-42}$, $z = 13.54$; Wilcoxon signed rank tests), indicating an increase in firing rate during both sleep stages compared to wake. Interneurons do not change firing rates between REM and wake (blue, monosynaptically identified interneurons, $n = 175$; REM/wake: $P = 0.21$, $z = 1.25$) and slightly decrease firing rates during NREM compared to wake (NREM/wake: $P = 1.97 \times 10^{-9}$, $z = -6.00$; Wilcoxon signed rank tests; dotted lines: medians).

3, 1,138; rat 4, 2,514). On the basis of histological reconstruction of probe placement and probe movement record, 2,038 of these were in the BLA, 782 in the central nuclei, 1,560 in the piriform cortex and 1,210 in the hippocampus (**Supplementary Table 1**). Units were further characterized as putative pyramidal cells and interneurons by waveform and physiological criteria (**Supplementary Fig. 3** and Online Methods). The firing rates of pyramidal cells followed a skewed distribution during sleep (NREM and REM) and wakefulness[31] (**Fig. 2c**). In addition, we found a specific increase in the firing rate of BLA pyramidal cells, but not interneurons, during REM sleep and, to a lesser extent, NREM sleep relative to wakefulness, as shown by the distributions of REM/wake or NREM/wake firing rate ratios for the two cell types (**Fig. 2c** and Online Methods).

BLA–hippocampus coordinated reactivations during NREM sleep

Reactivations across the hippocampus–amygdala network as well as within-structure networks (**Supplementary Fig. 4**) were quantified using the explained variance (EV). EV is the percentage of variance in the population of pairwise correlations during post-sleep (REM or NREM) that can be explained by run correlations ('reactivation') while taking into account pre-existing correlations during pre-sleep (REM or NREM[32–34]; **Fig. 3a,b** and Online Methods). The reverse explained variance (REV), calculated by switching the pre-sleep and post-sleep epochs, is used as a control value. The EV and REV, calculated using hippocampus–BLA pyramidal cell pairs, showed significant reactivations between the hippocampus and BLA during post-NREM (**Fig. 3c**). The gradual decay in reactivations over the first hour of NREM sleep (**Fig. 3c**; mean differences between EV and REV, ± s.e.m.: 0–20 min, 2.89 ± 0.47%; 20–40 min, 1.72 ± 0.44%; 40–60 min, 1.31 ± 0.60%; $n = 19$ sessions, $P = 0.014$, d.f. = 2, $\chi^2 = 8.53$; Kruskal-Wallis test) paralleled the previously described decay for pairs of hippocampal neurons[35,36]. Reactivations were maintained when both pyramidal cells and interneurons were included in the EV calculation (**Supplementary Fig. 5**). Neurons in the piriform cortex showed weaker experience-induced

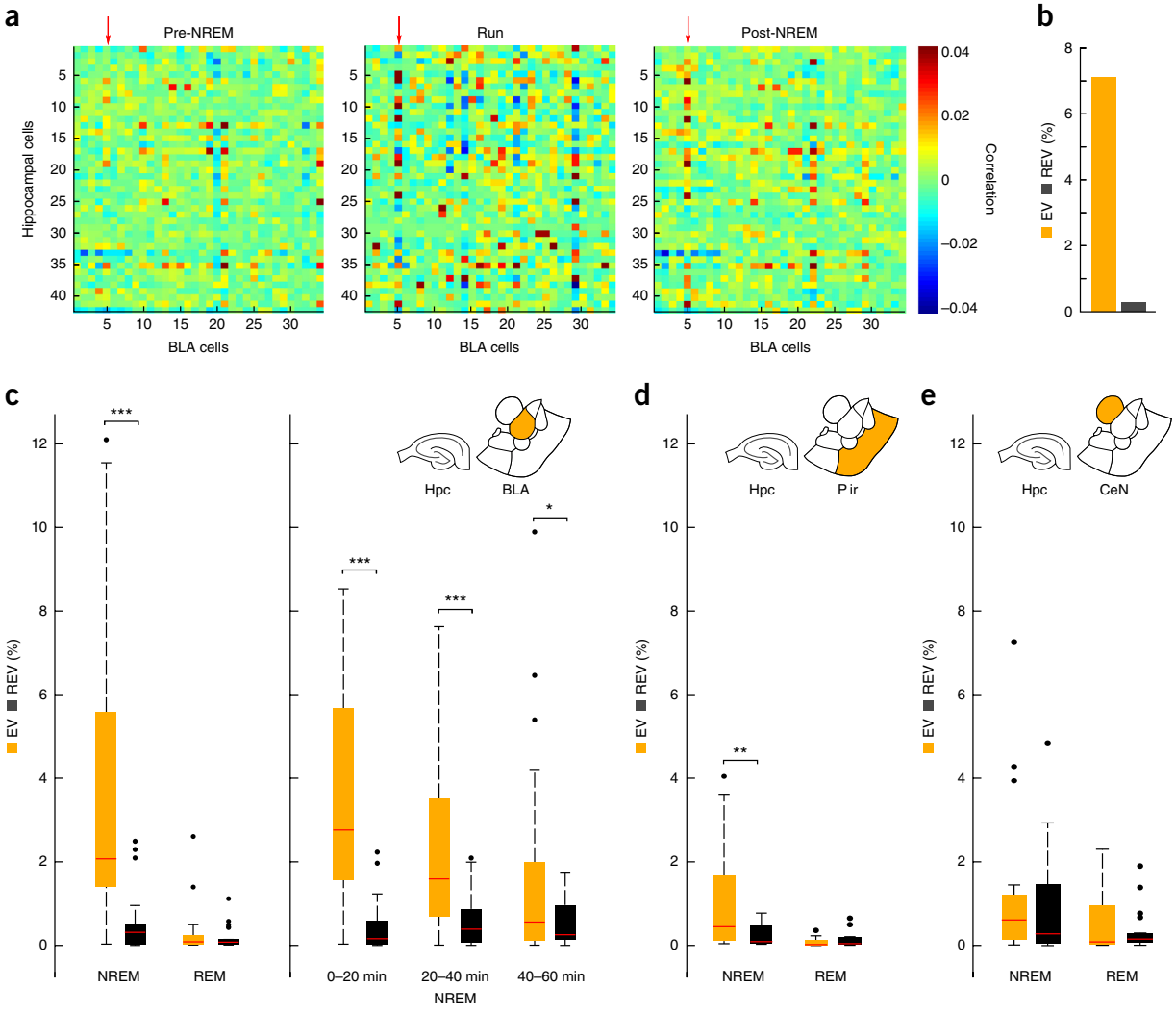

Figure 3 Hippocampus–BLA ensembles reactivate during NREM sleep. (**a**) Correlation matrices were calculated for hippocampus–BLA cell pairs for the pre-NREM, run and post-NREM epochs in 50-ms time bins. These matrices were used to calculate the explained variance (EV) and its control value, reverse explained variance (REV). Red arrows: strong coactivations of a single BLA pyramidal neuron with multiple hippocampal pyramidal (pyr) cells in an example session (1 animal and session out of 3 animals and 25 sessions for NREM sleep). (**b**) NREM EV and REV for the example session shown in **a**. (**c**) Left: EV and REV across all sessions for NREM ($n = 25$, $P = 0.00019$, $z = 3.72$; $n = 3$ rats) and REM sleep ($n = 23$, $P = 0.377$, $z = 0.88$; $n = 3$ rats; pyr–pyr pairs). Right: EV and REV for successive 20 min epochs of NREM for sessions where EV > REV in the first 20-min NREM epoch (pyr–pyr pairs; $n = 19$ sessions in 3 rats, 0–20 min: $P = 0.00013$, $z = 0.38$; 20–40 min: $P = 0.00046$, $z = 3.5$; 40–60 min: $P = 0.0312$, $z = 2.15$). (**d**) Hippocampus–piriform cortex EV and REV (NREM: $n = 17$ sessions, $P = 0.0052$; REM: $n = 15$ sessions in 3 rats, $P = 0.301$; pyr–pyr pairs). (**e**) Same as **d** but for central nuclei (CeN) (NREM: $n = 19$ sessions, $P = 0.717$, $z = 0.36$ and REM: $n = 19$ sessions, $P = 0.687$, $z = -0.40$; all cell pairs; $n = 3$ rats). All tests are Wilcoxon signed rank tests, $^{***}P < 0.001$, $^{**}P < 0.01$, $^{*}P < 0.05$. All box plots show the median (red line), first and last quartiles (box), and minimum and maximum values excluding outliers (whiskers), outliers (black dots).

reactivation with their CA1 partner neurons (**Fig. 3d**; Wilcoxon one-tailed rank sum test on EV – REV for hippocampus–BLA ($n = 25$ sessions, mean EV – REV 3.13 ± 0.73%, s.e.m.) vs. hippocampus–piriform cortex ($n = 14$, mean EV – REV 0.85 ± 0.34%, s.e.m.), $P = 0.0092$, $z = 2.38$), while there were no reactivations at all between the central nuclei and the hippocampus (**Fig. 3e**). Reactivations during REM sleep[27,37,38] were not significant in any structure, despite the robust REM-sleep-specific increase in BLA putative pyramidal cells firing rates (**Figs. 2c** and **3c–e** and **Supplementary Fig. 5a**).

A subset of BLA cells are modulated during hippocampal SPW-Rs

BLA neurons receive direct input from ventral, but not dorsal, CA1 neurons[22]. However, spatial location is more precisely coded by dorsal CA1 neurons than ventral ones[14,15]. Because both dorsal and ventral hippocampal neurons fire together during large-amplitude SPW-Rs[29], SPW-Rs may establish functional connections between the dorsal hippocampus and amygdala. To test this hypothesis, we examined the functional relationship between SPW-Rs and BLA neurons. A fraction of BLA neurons were significantly and positively modulated ('upmodulation'; 42 of 163 interneurons (25.8%), 137 of 1,233 pyramidal cells (11.1%)) or negatively modulated ('downmodulation'; 24 of 163 interneurons (14.7%), 102 of 1,233 pyramidal cells (8.3%)) during hippocampal SPW-Rs (**Fig. 4**). This confirmed the indirect influence of dorsal hippocampal SPW-Rs on BLA cells. Moreover, reactivations calculated using SPW-R-modulated BLA cells were larger than for nonmodulated pairs (**Supplementary Fig. 5b**).

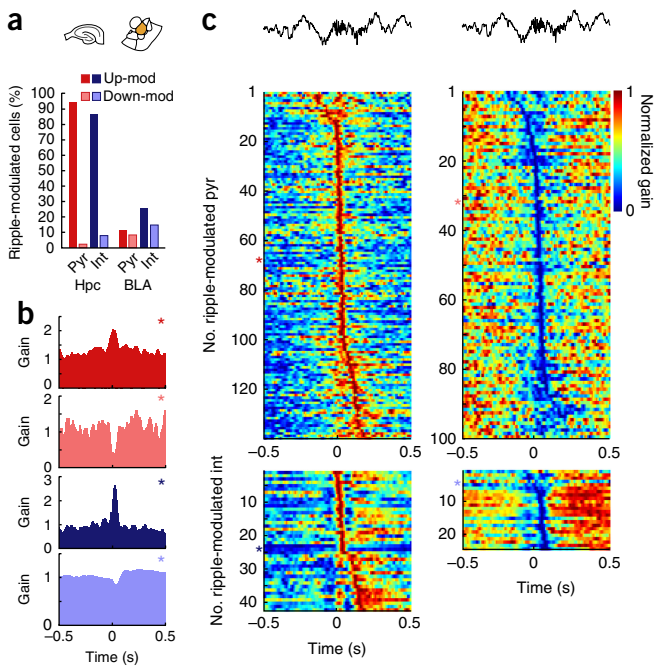

Figure 4 Subsets of BLA cells are up- or downmodulated during hippocampal SPW-Rs. (**a**) Percentages of hippocampal (Hpc) and BLA putative pyramidal cells (pyr; red) and interneurons (int; blue) that are significantly upmodulated (up-mod; dark red or dark blue) or downmodulated (down-mod; light red or light blue) during SPW-Rs (Hpc: $n = 41$ sessions, $n = 3$ rats; BLA: $n = 29$ sessions, $n = 3$ rats). (**b**) Peri-event gain for two putative BLA pyramidal cells (red: top, upmodulated; bottom, downmodulated) and interneurons (blue: top, upmodulated; bottom, downmodulated). These neurons are indicated by the respective colored asterisks in **c**. (**c**) Normalized peri-event gain for all upmodulated (top left) and downmodulated (top right) BLA putative pyramidal cells (top panels) and interneurons (bottom panels). Top black traces: example hippocampal ripples (LFP).

Ripple-modulated BLA cells are preferentially involved in reactivations

In a further attempt to characterize the reactivation dynamics during sleep, we used two complementary approaches. In the first approach, we defined the firing properties of individual neurons relative to ripples and then examined how such properties influenced reactivations. The second approach worked from the opposite direction. First, we quantified reactivations for each cell irrespective of their LFP ripple correlates and examined how their reactivation values were related to ripples. During run, a fraction of hippocampal–BLA pyramidal neuron pairs showed significantly positively correlated spike trains (2,521 of 37,660; 6.69%). Another small percentage (1,258 of 37,660; 3.34%) was negatively correlated, while the remaining majority (33,881 of 37,660; 89.96%) was not reliably correlated (Online Methods; total number of pyramidal–pyramidal hippocampus–BLA pairs 37,660: rat 1, 16,056; rat 3, 3,836; rat 4, 17,768). To test whether a selective subgroup of pairs was preferentially involved in sleep reactivations, we separated pairs into nine subgroups based on a combination of run correlation and SPW-R modulation of the BLA partner (**Fig. 5a**, **Supplementary Fig. 6** and **Supplementary Table 2**). Hippocampus–BLA pairs with significant, positive run correlations and SPW-R upmodulation of the BLA partner showed the largest pre-NREM to post-NREM change (one-way ANOVA, $P = 1.1 \times 10^{-45}$, d.f. = 8, $F = 29.09$; *post hoc* comparisons, $P < 0.001$). The dominant contribution of this specific subgroup of cell pairs to reactivations was confirmed by calculating the EVs across the nine subgroups (pairs grouped across animals and sessions; **Supplementary Fig. 6b**).

In the second approach, we evaluated the contribution of each cell pair to the overall EV (calculated with all pairs across animals and sessions) by removing hippocampus–BLA pairs one by one. The change in EV ($EV^{all} - EV^{minus\ one\ pair}$) indicates the individual contribution of the removed pair (the larger the decrease in EV, the larger the contribution of the pair; **Supplementary Fig. 7a**). To obtain a per-cell contribution measure, contributions were averaged over all the pairs that the cell participated in. We then divided BLA cells into quartiles according to the magnitude of their individual contributions. We found that upmodulated BLA neurons in the most strongly contributing quartile showed a specific increase in SPW-R gain (that is, firing rate during versus outside SPW-R) from pre-NREM to post-NREM compared to the upmodulated cells of the remaining three, low-contribution quartiles (**Fig. 5b** and **Supplementary Fig. 8**; Wilcoxon one-tail sign-rank test on gain averaged in a 500-ms window around ripple peak; high-contribution quartile: $P = 4.57 \times 10^{-5}$, $z = 3.91$; low-contribution quartiles: $P = 0.991$, $z = 2.40$). To control for the effects of firing rates, we calculated EVs and REVs for pairs pooled according to their firing rates (individual BLA cell firing rate, hippocampal cell firing rate or combined firing rate). This control showed that EV did not depend on firing rates (**Supplementary Fig. 9**).

The aversive trajectory is reactivated during SPW-Rs

BLA cells that are upmodulated during hippocampal ripples show a preferential involvement in coordinated reactivations, through an increased gain of their modulation after training. However, these observations offer only indirect support for reactivations during hippocampal SPW-Rs. Furthermore, these findings alone do not directly address the critical role of threat in sleep reactivations. To obtain more direct support, we used a reactivation strength (R) measure (**Supplementary Fig. 10** and Online Methods) and analyzed firing patterns separately during the two directions of travel. Since the air puff was presented during only one direction of run on the track (air puff or danger trajectory) on a given day, the opposite run can be considered safe. Therefore, we compared the reactivation strengths of the hippocampus–BLA pairwise correlation patterns of the air puff vs. the safe direction. We found that the reinstatement of the joint hippocampus–BLA neuron representation was significantly enhanced during post-NREM SPW-R compared to pre-NREM SPW-Rs for the air puff direction but not for the safe direction (**Fig. 6a**,**b** and **Supplementary Fig. 11b**,**c**). Because the firing rates of BLA cells did not significantly differ between safe and air puff trajectories (pyramidal cells: $P = 0.270$, $z = 1.101$; all cells: $P = 0.763$, $z = 0.302$, Wilcoxon signed rank tests), the reactivation results cannot be explained by air-puff-induced firing rate increase. The occurrence rate of SPW-R was also not significantly different between the pre-NREM and post-NREM epochs ($P = 0.192$; $z = -1.289$, $n = 41$ sessions; Wilcoxon signed rank test; **Supplementary Fig. 11d**). These observations thus confirm that NREM sleep SPW-Rs are specific time windows within which the place–threat association is reinstated during sleep.

NREM contributes to reinstatement of new place–threat representations

Finally, we examined how sleep reactivations are linked to the place–threat representation during wakefulness. Rats learned a new air puff location every day during the training session (**Fig. 1a**,**b**).

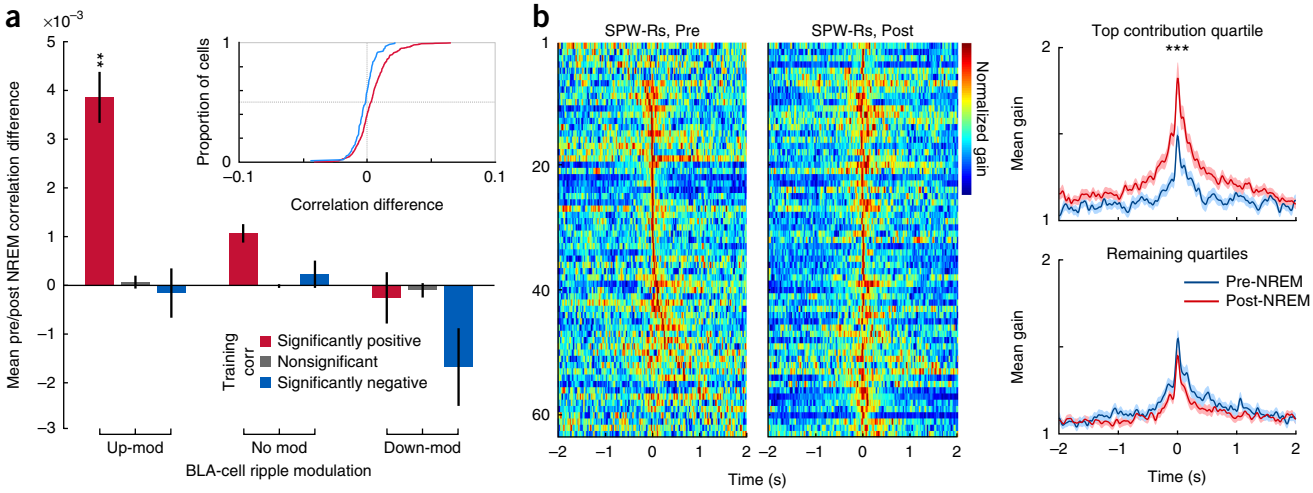

Figure 5 Reactivations rely on pairs with correlated activity during run and a BLA partner that is upmodulated during hippocampal SPW-Rs. Strongly contributing modulated BLA cells selectively increase their gain during SPW-Rs following training. (**a**) Mean differences between pre-NREM and post-NREM correlations for each group of cell pairs classified according to (i) the ripple-modulation type of the BLA cell—upmodulation (up-mod), no modulation (no mod) or downmodulation (down-mod)—and (ii) the correlation during the run—significantly positive, nonsignificant or significantly negative. Inset shows the normalized cumulative distributions of the post-NREM – pre-NREM correlation difference for the upmodulated, significantly positive run correlation group (red) and downmodulated, significantly negative run correlation group (blue; error bars: s.e.m.; $n = 37{,}660$ pairs, one-way ANOVA $P = 1.1 \times 10^{-45}$, d.f. = 8, $F = 29.09$, $n = 3$ rats). The upmodulated, significantly positive correlation group is the only one to be significantly different from all others (*post hoc* Tukey–Kramer multiple comparison test with $^{**}P < 0.01$). Details of all distributions are shown in **Supplementary Figure 6.** (**b**) Left: peri-ripple gains for upmodulated cells of the highly contributing quartile for pre-NREM SPW-Rs and post-NREM SPW-Rs (color: normalized gain per cell; cells are sorted by timing of the bin with highest gain during the pre-sleep epoch). Right: mean (± s.e.m.) gain during pre-NREM (blue) and post-NREM (red) SPW-Rs for upmodulated cells of the strongly contributing quartile (top) and for the remaining quartiles (bottom). There is a significant increase in gain between pre-NREM and post-NREM SPWRs for strongly contributing BLA upmodulated cells (Wilcoxon one-tail signed rank tests on gain averaged in a 500-ms window around ripple peak; high contribution quartiles: $n = 63$ cells, $^{***}P = 4.57 \times 10^{-5}$, $z = -3.913$; low contribution quartiles: $n = 73$ cells, $P = 0.992$, $z = 2.408$; $n = 3$ rats).

The joint representation of space and threat is thus expected to be different between the pre-run test, when the new location has not been experienced yet, and the post-run test, when it has been experienced and replayed during sleep. **Figure 7a** shows examples of highly contributing BLA–hippocampus cell pairs that showed air-puff-related activity (BLA) and air-puff-related place fields (hippocampus). These coordinated patterns developed during training and were maintained in the post-run test in the absence of an air puff. To quantify this relationship, we examined separately the most strongly contributing pairs (represented by the highest 2.5th percentile of the contribution distribution) and the least strongly contributing pairs (the 2.5th percentile of lowest contribution; **Supplementary Fig. 7b**). We found that for strongly contributing, but not for weakly contributing, pairs the increase between pre-run and post-run coactivity was significantly correlated with the increase in coactivity between pre-NREM and post-NREM (**Fig. 7b**). This result was maintained when the most strongly and the most weakly contributing quartiles (instead of 2.5th percentiles) of the distribution were compared (**Fig. 7c**). These coordinated changes indicate that reactivations during sleep play a role in the stabilization of the new space–threat representation.

DISCUSSION

We found that correlated neuronal activity between neurons of the dorsal hippocampus and BLA was strengthened during NREM sleep following experience in a spatially anchored threat model[39,40]. Reactivations involved a subgroup of hippocampus-responsive neurons in BLA and occurred in association with hippocampal SPW-Rs. Notably, the reactivation of hippocampus–BLA coactivity during post-experience sleep was stronger for the patterns of pairwise correlations dominating during the travel through the danger zone, compared to reactivations of the pairwise patterns representing the safe direction.

Previous works have shown that in both spatial memory tasks and contextual threat learning only a small set of neurons is active in the hippocampus and amygdala[7–9,35]. Identifying amygdala neurons that receive hippocampal inputs required recording from an unprecedentedly large number of individual neurons simultaneously in these two structures. We achieved this by using multi-shank silicon probes and an experimental design that allowed us to generate new place–threat associations every day so that we could slowly advance our probes through the full structure of the amygdala and sample new sets of neurons daily. Of the large number of cross-structure neuron pairs, we identified the relevant subset whose coactivation increased significantly from pre-experience to post-experience sleep and thus contributed to the cross-structure reactivations. We further characterized the amygdala members of these pairs as hippocampus-responding because they increased firing rates during hippocampal SPW-Rs. In contrast, BLA neurons that decreased or did not change their activity during SPW-Rs did not show significant change in their correlation with hippocampal neuron partners from pre-experience to post-experience sleep. Furthermore, neuron pairs across the hippocampus and BLA that showed the strongest increase in correlation from pre-experience sleep to post-experience sleep were those that also showed the strongest correlations during learning of the place–threat association. For the reactivated pairs only, the changes in the strength of coactivation during sleep induced by training were correlated with the changes in the coactivations on the test sessions on

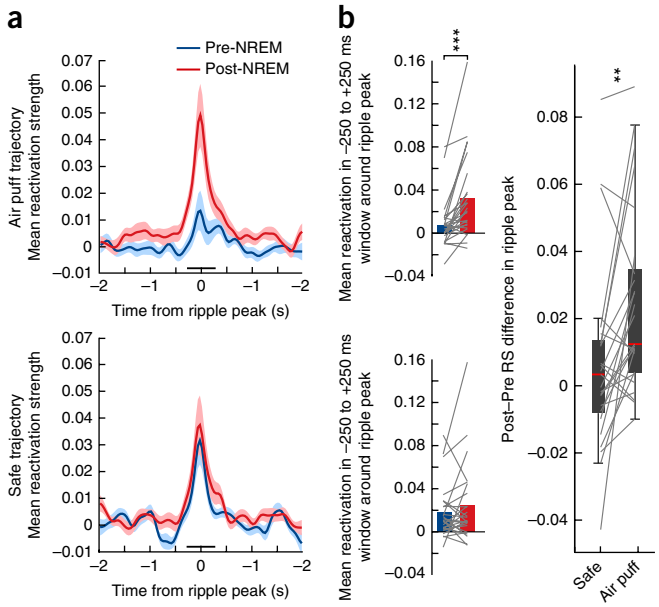

Figure 6 Hippocampus–BLA reactivations of the air puff trajectory peak during hippocampal SPW-Rs. (**a**) Mean (± s.e.m.) *z*-scored peri-ripple reactivation strength of the air puff (top) versus safe (bottom) trajectories over animals ($n = 3$) and sessions ($n = 25$) for pre-NREM (blue) and post-NREM (red) hippocampal SPW-Rs. Right: reactivation strength in a 500-ms window around ripple peaks (gray bars) was significantly higher in post-NREM compared to pre-NREM for air puff trajectory (***$P = 7.42 \times 10^{-5}$, $z = -3.793$), but not for safe trajectory ($P = 0.217$, $z = -0.780$; Wilcoxon one-tail signed rank tests). Gray lines from pre-NREM to post-NREM indicate single sessions. (**b**) The pre-NREM vs. post-NREM difference in reactivation strength (RS) at the ripple peak is significantly higher for the air puff trajectory compared to safe trajectory (Wilcoxon one-tail signed rank-test; **$P = 0.00257$, $z = -2.798$, $n = 25$ sessions; box plots show the median (red line), first and last quartiles (box), and minimum and maximum values (whiskers) excluding outliers).

the track. Moreover, experience-induced reactivations were stronger for hippocampus–BLA pairs correlated during travel that involved the aversive air puff, compared to travel in the safe direction. Overall, our findings suggest that training on the place–threat association creates a novel joint representation between the hippocampus and the amygdala that is subsequently consolidated or reconsolidated during sleep and is reinstated on the track during the test session in absence of the threat.

The dorsal hippocampus is crucially involved in spatial memory, including classical context–threat associations[19,41], in line with the observations that neurons in the dorsal hippocampus carry highly specific spatial information[13]. More specifically, it has been shown that the indirect suppression of sleep hippocampal SPW-Rs, known to consolidate spatial memories[24], impairs contextual fear conditioning[25]. By comparison, the importance of the ventral hippocampus for contextual processing is debated[42], again in line with the coarser spatial representation of ventral hippocampal neurons[14,15]. We show that despite the lack of direct connections from dorsal hippocampus to BLA, a fraction of BLA pyramidal cells and interneurons were effectively entrained by SPW-Rs of the dorsal hippocampus. We hypothesize that this is possible because during large amplitude SPW-Rs populations of the dorsal and ventral hippocampus, likely involving ventral neurons projecting to the amygdala[43], robustly synchronize. Indeed, one postulated role of SPW-Rs is to combine neuronal activity across different segments of the hippocampus[29,44] that send and receive projections to different parts of the neocortex, amygdala and subcortical structures[45].

Alternative explanations should also be considered. In addition to the direct ventral hippocampus–amygdala projections, a hippocampus–entorhinal cortex–amygdala route may also be involved, given that BLA–entorhinal connections have been implicated in the acquisition of contextual threat conditioning[46] and given that deep-layer entorhinal neurons also respond robustly to SPW-Rs[47]. Another potential explanation for the hippocampus–amygdala sleep replay is that both neuronal populations are simply responding to a third party, such as slow oscillations. However, several findings argue against this possibility. First, neuronal responses in BLA to hippocampal SPW-Rs were immediate and short. If firing correlations were driven by UP-DOWN states of sleep or spindles, more prolonged firing rate responses would be expected. Second, DOWN-UP shift induces increases but not decreases in firing rates. In contrast, a large fraction of the amygdala neurons responded with suppression of firing rates during hippocampal SPW-R. Third, only SPW-R-excited BLA neurons showed a significant change from pre-experience to post-experience sleep. Conversely, we found that BLA neurons with high contribution to reactivations were more likely to increase their association with SPW-R during sleep after learning compared to sleep before learning. Overall, our findings suggest that SPW-Rs are instrumental for establishing functional connections between dorsal hippocampus and BLA to consolidate place–threat associations.

Previous findings in humans and other animals have suggested that REM sleep is critical for the consolidation of emotional information[27,36,37,48,49]. Our results showing an elevated firing rate of BLA pyramidal cells during REM sleep are in line with this hypothesis. However, we did not find significant reactivations during REM sleep. The short duration of REM sleep episodes and the consequently low number of spikes available for the analyses we performed may contribute to the lack of significant reactivations during REM sleep. It is also possible that REM sleep plays a different or complementary role in the consolidation of emotional memories that does not involve an offline reinstatement of the joint hippocampus–BLA representation. Finally, our work did not address the potential role of subcortical neurotransmitters in memory replay and consolidation[50] or the role of the entorhinal cortex as a possible mediator of information exchange between hippocampus and amygdala. These questions remain to be answered by future investigations.

In summary, we identified a small subset of hippocampus–BLA neuronal pairs that are reactivated during sleep SPW-Rs following training in a place–threat association task. The BLA partners of these pairs are preferentially upmodulated during SPW-Rs and selectively increase their firing rate during SPW-Rs after training. This finding suggests that SPW-R replay provides a physiological mechanism to integrate place cell activity in the dorsal hippocampus and threat-responsive neurons in the amygdala. We hypothesize that concerted activation of hippocampal and BLA cells during SPW-Rs is responsible for combining spatial/contextual and emotional representations during NREM sleep and thus for the consolidation of contextual fear. Direct support for this hypothesis will require further experiments, such as dynamic perturbation of BLA neurons specifically during SPW-Rs.

METHODS

Methods, including statements of data availability and any associated accession codes and references, are available in the online version of the paper.

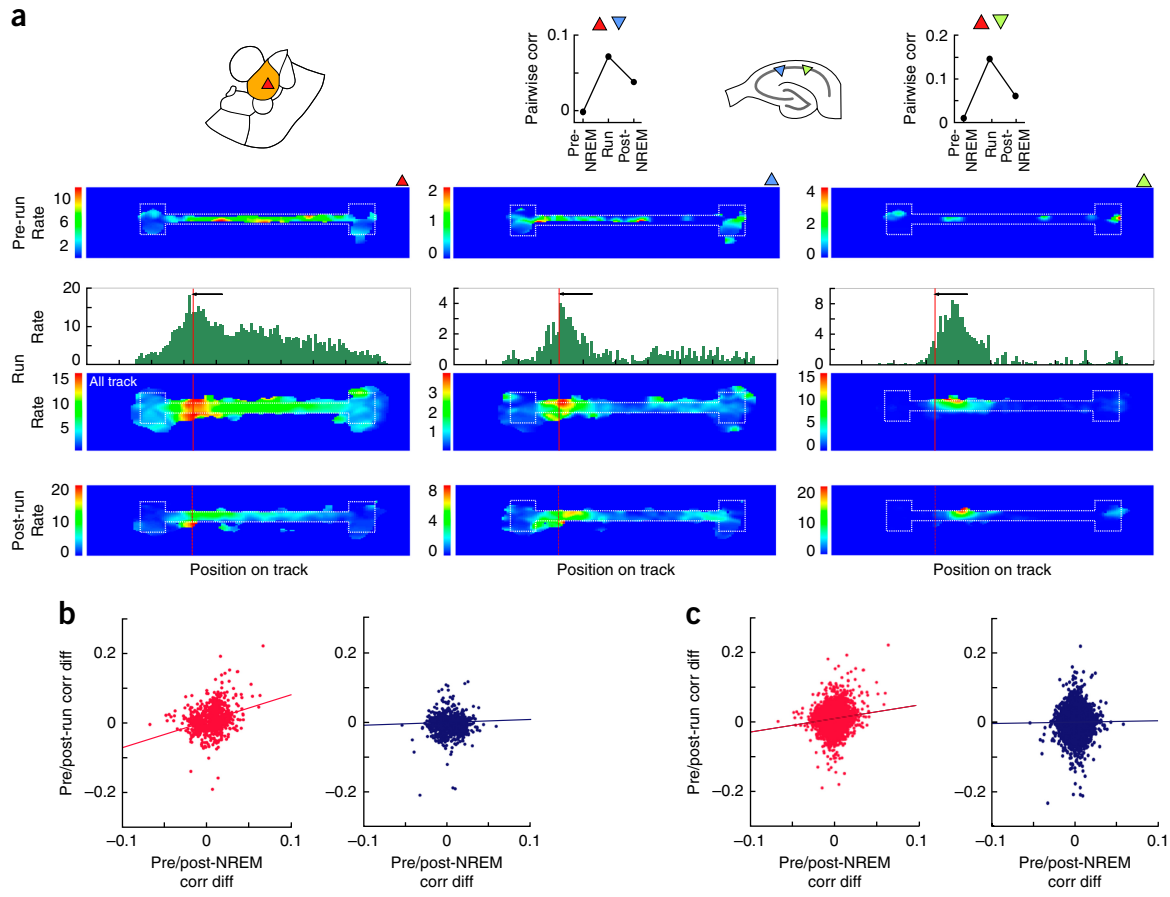

Figure 7 Contributing pairs form a representation during the run that is reactivated during sleep and reinstated during post-run without the air puff. (**a**) Behavioral correlates of an example BLA pyramidal cell (left; red triangle) that forms highly contributing pairs with two hippocampal place cells (center and right; blue and green triangles). Firing maps are shown for pre-run, run and post-run epochs (top to bottom) and firing rate histogram for run. Red line: air puff location. Black arrows: running direction in which the air puff is applied ('air puff trajectory'). Color bars are in hertz. (**b**) Correlation between changes in pre vs. post-NREM correlations and pre- vs. post-run correlations for strongly contributing pairs (red, 2.5% highest contributions) and weakly contributing pairs (blue, 2.5% lowest contributions). NREM and run changes are correlated for strongly contributing pairs (Pearson $r = 0.27$, $n = 866$ pairs, $P = 2.11 \times 10^{-16}$; $n = 3$ rats), but not for weakly contributing pairs ($r = 0.03$, $n = 845$ pairs, $P = 0.305$; $n = 3$ rats). Corr diff, correlation difference. (**c**) Same as **b** but for strong ($n = 9{,}415$ pairs, $r = 0.13$, $P = 1.07 \times 10^{-32}$; $n = 3$ rats) and weak ($n = 9{,}415$ pairs, $r = 0.013$, $P = 0.22$; $n = 3$ rats) contributing quartiles (25% highest and lowest contributions).

Note: Any Supplementary Information and Source Data files are available in the online version of the paper.

ACKNOWLEDGMENTS

We thank J. LeDoux, C. Léna, E. Stark, A. Peyrache and L. Roux for comments and discussions on the analyses and manuscript and all the members of the Buzsáki laboratory for their support. This work was supported by the Fondation pour la Recherche Médicale (FRM), the Fyssen Foundation, a Charles H. Revson Senior Fellowship in Biomedical Science (G.G.), NIH MH54671 and MH107396, NS 090583 and the Simons Foundations (G.B.).

AUTHOR CONTRIBUTIONS

G.G. and G.B. designed the study, G.G. and I.I. performed the experiments, G.G. analyzed the data and G.B. and G.G. wrote the manuscript.

COMPETING FINANCIAL INTERESTS

The authors declare no competing financial interests.

1. Vazdarjanova, A. & McGaugh, J.L. Basolateral amygdala is involved in modulating consolidation of memory for classical fear conditioning. *J. Neurosci.* **19**, 6615–6622 (1999).
2. Paré, D., Collins, D.R. & Pelletier, J.G. Amygdala oscillations and the consolidation of emotional memories. *Trends Cogn. Sci.* **6**, 306–314 (2002).
3. Maren, S. & Fanselow, M.S. Synaptic plasticity in the basolateral amygdala induced by hippocampal formation stimulation in vivo. *J. Neurosci.* **15**, 7548–7564 (1995).
4. Ikegaya, Y., Saito, H. & Abe, K. Attenuated hippocampal long-term potentiation in basolateral amygdala-lesioned rats. *Brain Res.* **656**, 157–164 (1994).
5. Ikegaya, Y., Saito, H. & Abe, K. High-frequency stimulation of the basolateral amygdala facilitates the induction of long-term potentiation in the dentate gyrus in vivo. *Neurosci. Res.* **22**, 203–207 (1995).
6. Goshen, I. *et al.* Dynamics of retrieval strategies for remote memories. *Cell* **147**, 678–689 (2011).
7. Reijmers, L.G., Perkins, B.L., Matsuo, N. & Mayford, M. Localization of a stable neural correlate of associative memory. *Science* **317**, 1230–1233 (2007).
8. Redondo, R.L. *et al.* Bidirectional switch of the valence associated with a hippocampal contextual memory engram. *Nature* **513**, 426–430 (2014).
9. Hsiang, H.-L.L. *et al.* Manipulating a "cocaine engram" in mice. *J. Neurosci.* **34**, 14115–14127 (2014).
10. Xu, C. *et al.* Distinct hippocampal pathways mediate dissociable roles of context in memory retrieval. *Cell* **167**, 961–972 (2016).
11. Phillips, R.G. & LeDoux, J.E. Differential contribution of amygdala and hippocampus to cued and contextual fear conditioning. *Behav. Neurosci.* **106**, 274–285 (1992).

12. Zelikowsky, M., Hersman, S., Chawla, M.K., Barnes, C.A. & Fanselow, M.S. Neuronal ensembles in amygdala, hippocampus, and prefrontal cortex track differential components of contextual fear. *J. Neurosci.* **34**, 8462–8466 (2014).
13. O'Keefe, J. & Nadel, L. *The Hippocampus as a Cognitive Map* (Oxford Univ. Press, 1978).
14. Kjelstrup, K.G. *et al.* Reduced fear expression after lesions of the ventral hippocampus. *Proc. Natl. Acad. Sci. USA* **99**, 10825–10830 (2002).
15. Royer, S., Sirota, A., Patel, J. & Buzsáki, G. Distinct representations and theta dynamics in dorsal and ventral hippocampus. *J. Neurosci.* **30**, 1777–1787 (2010).
16. Moser, M.B., Moser, E.I., Forrest, E., Andersen, P. & Morris, R.G. Spatial learning with a minislab in the dorsal hippocampus. *Proc. Natl. Acad. Sci. USA* **92**, 9697–9701 (1995).
17. Moser, E.I.E., Krobert, K.A., Moser, M.B. & Morris, R.G. Impaired spatial learning after saturation of long-term potentiation. *Science* **281**, 2038–2042 (1998).
18. Small, S.A. The longitudinal axis of the hippocampal formation: its anatomy, circuitry, and role in cognitive function. *Rev. Neurosci.* **13**, 183–194 (2002).
19. Kim, J.J. & Fanselow, M.S. Modality-specific retrograde amnesia of fear. *Science* **256**, 675–677 (1992).
20. Corcoran, K.A., Desmond, T.J., Frey, K.A. & Maren, S. Hippocampal inactivation disrupts the acquisition and contextual encoding of fear extinction. *J. Neurosci.* **25**, 8978–8987 (2005).
21. Maren, S. & Quirk, G.J. Neuronal signalling of fear memory. *Nat. Rev. Neurosci.* **5**, 844–852 (2004).
22. Pitkänen, A., Pikkarainen, M., Nurminen, N. & Ylinen, A. Reciprocal connections between the amygdala and the hippocampal formation, perirhinal cortex, and postrhinal cortex in rat. A review. *Ann. NY Acad. Sci.* **911**, 369–391 (2000).
23. Herry, C. *et al.* Switching on and off fear by distinct neuronal circuits. *Nature* **454**, 600–606 (2008).
24. Girardeau, G. & Zugaro, M. Hippocampal ripples and memory consolidation. *Curr. Opin. Neurobiol.* **21**, 452–459 (2011).
25. Wang, D.V. *et al.* Mesopontine median raphe regulates hippocampal ripple oscillation and memory consolidation. *Nat. Neurosci.* **18**, 728–735 (2015).
26. van de Ven, G.M., Trouche, S., McNamara, C.G., Allen, K. & Dupret, D. Hippocampal offline reactivation consolidates recently formed cell assembly patterns during sharp wave-ripples. *Neuron* **92**, 968–974 (2016).
27. Popa, D., Duvarci, S., Popescu, A.T., Léna, C. & Paré, D. Coherent amygdalocortical theta promotes fear memory consolidation during paradoxical sleep. *Proc. Natl. Acad. Sci. USA* **107**, 6516–6519 (2010).
28. Huff, M.L., Miller, R.L., Deisseroth, K., Moorman, D.E. & LaLumiere, R.T. Posttraining optogenetic manipulations of basolateral amygdala activity modulate consolidation of inhibitory avoidance memory in rats. *Proc. Natl. Acad. Sci. USA* **110**, 3597–3602 (2013).
29. Patel, J., Schomburg, E.W., Berényi, A., Fujisawa, S. & Buzsáki, G. Local generation and propagation of ripples along the septotemporal axis of the hippocampus. *J. Neurosci.* **33**, 17029–17041 (2013).
30. Lovett-Barron, M. *et al.* Dendritic inhibition in the hippocampus supports fear learning. *Science* **343**, 857–863 (2014).
31. Mizuseki, K., Royer, S., Diba, K. & Buzsáki, G. Activity dynamics and behavioral correlates of CA3 and CA1 hippocampal pyramidal neurons. *Hippocampus* **22**, 1659–1680 (2012).
32. Kudrimoti, H.S., Barnes, C.A. & McNaughton, B.L. Reactivation of hippocampal cell assemblies: effects of behavioral state, experience, and EEG dynamics. *J. Neurosci.* **19**, 4090–4101 (1999).
33. Lansink, C.S., Goltstein, P.M., Lankelma, J.V., McNaughton, B.L. & Pennartz, C.M.A. Hippocampus leads ventral striatum in replay of place-reward information. *PLoS Biol.* **7**, e1000173 (2009).
34. Hoffman, K.L. & McNaughton, B.L. Coordinated reactivation of distributed memory traces in primate neocortex. *Science* **297**, 2070–2073 (2002).
35. Wilson, M. & McNaughton, B. Reactivation of hippocampal ensemble memories during sleep. *Science (80-)* **5**, 14–17 (1994).
36. Shen, J., Kudrimoti, H.S., McNaughton, B.L. & Barnes, C.A. Reactivation of neuronal ensembles in hippocampal dentate gyrus during sleep after spatial experience. *J. Sleep Res.* **7** (Suppl. 1), 6–16 (1998).
37. Genzel, L., Spoormaker, V.I., Konrad, B.N. & Dresler, M. The role of rapid eye movement sleep for amygdala-related memory processing. *Neurobiol. Learn. Mem.* **122**, 110–121 (2015).
38. Hutchison, I.C. & Rathore, S. The role of REM sleep theta activity in emotional memory. *Front. Psychol.* **6**, 1439 (2015).
39. LeDoux, J.E. Coming to terms with fear. *Proc. Natl. Acad. Sci. USA* **111**, 2871–2878 (2014).
40. Moita, M.A., Rosis, S., Zhou, Y., LeDoux, J.E. & Blair, H.T. Putting fear in its place: remapping of hippocampal place cells during fear conditioning. *J. Neurosci.* **24**, 7015–7023 (2004).
41. Wang, M.E. *et al.* Differential roles of the dorsal and ventral hippocampus in predator odor contextual fear conditioning. *Hippocampus* **23**, 451–466 (2013).
42. Bannerman, D.M. *et al.* Regional dissociations within the hippocampus—memory and anxiety. *Neurosci. Biobehav. Rev.* **28**, 273–283 (2004).
43. Ciocchi, S., Passecker, J., Malagon-Vina, H., Mikus, N. & Klausberger, T. Brain computation. Selective information routing by ventral hippocampal CA1 projection neurons. *Science* **348**, 560–563 (2015).
44. Buzsáki, G. Hippocampal sharp wave-ripple: a cognitive biomarker for episodic memory and planning. *Hippocampus* **25**, 1073–1188 (2015).
45. Logothetis, N.K. *et al.* Hippocampal–cortical interaction during periods of subcortical silence. *Nature* **491**, 547–553 (2012).
46. Sparta, D.R. *et al.* Inhibition of projections from the basolateral amygdala to the entorhinal cortex disrupts the acquisition of contextual fear. *Front. Behav. Neurosci.* **8**, 129 (2014).
47. Chrobak, J.J. & Buzsáki, G. High-frequency oscillations in the output networks of the hippocampal-entorhinal axis of the freely behaving rat. *J. Neurosci.* **16**, 3056–3066 (1996).
48. Boyce, R., Glasgow, S.D., Williams, S. & Adamantidis, A. Causal evidence for the role of REM sleep theta rhythm in contextual memory consolidation. *Science (80-)* **23**, 812 (2016).
49. Maquet, P. *et al.* Experience-dependent changes in cerebral activation during human REM sleep. *Nat. Neurosci.* **3**, 831–836 (2000).
50. Atherton, L.A., Dupret, D. & Mellor, J.R. Memory trace replay: the shaping of memory consolidation by neuromodulation. *Trends Neurosci.* **38**, 560–570 (2015).

ONLINE METHODS

Subjects and electrode implantation. All experiments were approved by the Institutional Animal Care and Use Committee (IACUC) at New York University Medical Center. Four individually housed male Long-Evans rats were used in this experiment, and maintained on a 12h:12h light-dark cycle (lights on at 7 a.m.) throughout the study. Animals (300 g, 3 months old at time of surgery) were deeply anesthetized with isoflurane. Three silicon probes (2 with 8 shanks, 1 with 4 shanks, 160 recording channels total, NeuroNexus H32 and H62, A-style, Buzsaki32 and 64 layout) mounted on individual movable microdrives[51] were implanted above the amygdalae bilaterally (AP −2.5 mm ML ± 3.6 to 5.5 mm from bregma) and in the dorsal hippocampus (left or right, CA1, AP −3.5 mm, ML ± 2.5 mm). The drives were secured to the skull using dental cement. Skull screws above the cerebellum were used as ground and reference. The drives and probes were protected by a cement-covered copper-mesh Faraday cage on which the probe connectors were attached. Animals were allowed to recover for at least 5 d with *ad libitum* food and water. In one animal, the hippocampus probe failed during the course of the experiment. This animal was hence not used for analysis about hippocampus–BLA coordination, but was used for intra-amygdala and intra-piriform cortex physiology and reactivation analysis. Data collection and analysis we not performed blind to the conditions of the experiments.

Recordings and behavior. All animals were free from prior manipulation before being included in the study. After a week of daily handling, animals were placed on water restriction and trained to run back and forth on a linear track for water rewards (**Fig. 1**). All experiments were performed during the day (light cycle). Three days before surgery, they regained access to *ad libitum* food and water. After the recovery period, the probes were slowly lowered in the brain and the recordings started when reaching hippocampal CA1 pyramidal layer and the superior limit of BLA, respectively. During this period, the rats were placed back on water restriction to >85% of their normal weight and re-exposed to the linear track. The position of the animal was tracked using a camera mounted on the ceiling and a red LED attached to the head of the animal. Signals were recorded at 20 kHz using an Amplipex recording system (Amplipex Inc., Szeged, Hungary) and the associated Amplirec software. The amygdala electrodes were lowered by 140 µm at the end of each recording session to ensure a complete spanning of the amygdala region over the course of the experiment. The hippocampal probe was adjusted daily to optimize ripple and unit recording.

Preprocessing. 20-kHz signals were resampled at 1,250 Hz to extract LFP data. Spikes were extracted by high-pass filtering (800 Hz) and thresholding the signal, then clustered using Klustakwik (http://sourceforge.net/projects/klustakwik/) followed by manual clustering using Klusters (http://neurosuite.sourceforge.net/) Data were visualized and preprocessed using Neuroscope (http://neurosuite.sourceforge.net/) and NDManager (http://neurosuite.sourceforge.net/)[52]. Units were classified into putative pyramidal cells and putative interneurons using monosynaptic connections (**Supplementary Fig. 3**). The remaining, unidentified cells were sorted using *k*-means clustering (two clusters) on the inverse frequency (that is, duration; fast Fourier transform) and peak-to-trough values (in milliseconds) of the mean waveform of the spikes. Sleep stages were manually scored through visual inspection of the hippocampus and amygdala spectrograms and accelerometer signal using the visual scoring custom program TheStateEditor. Periods of NREM were associated with immobility and high theta/delta ratio (in hippocampus) or gamma (45–65 Hz)/broad low frequency (1–12 Hz) band ratio (in amygdala). REM sleep was characterized by sleep posture and regular theta waves.

Statistical analysis. Non-parametric Wilcoxon rank sum or signed rank sum (two-tailed, unless otherwise specified) tests were used throughout the paper. All tests used are specified in the figure legends or in the text. Sample sizes were not predetermined, but our sample sizes are similar to (*n* animals) or higher than (*n* cells) those generally employed in the field. When parametric tests were used, the data satisfied the criteria for normality (Kolmogorov–Smirnov test) and equality of variance (Bartlett's test for equal variance). For multiple comparisons in the *post hoc* tests, the original *P*-values are shown but the significance thresholds $^{*}P < 0.05$, $^{**}P < 0.01$, $^{***}P < 0.001$ are indicated with either a Bonferroni corrections or Tukey–Kramer test for multiple comparisons. All data are represented with box plots showing the median with central and dispersion statistics. Some extreme data points are not shown in the figures for clarity but all data points were included in the analyses. Bar plots (**Fig. 5a**) are shown only in combination with the full distributions (**Supplementary Fig. 6**). *P*-values for Pearson's correlations are computed using a Student's *t* distribution for a transformation of the correlation (Matlab "corr" function). A **Life Sciences Reporting Summary** is available for an overview of ethics and statistics.

Analysis. All analyses were performed using Chronux (http://chronux.org/), the FMAToolbox (http://fmatoolbox.sourceforge.net/) and Matlab (The MathWorks, Inc., Natick, MA, USA) built-in functions and custom-written scripts.

For behavioral measures, speed ratios were calculated as (pDZ speed – cDZ speed)/(pDZ speed + cDZ speed), with pDZ the previous danger zone (20 cm preceding the air puff location of the previous training day) and cDZ the current danger zone (20 cm preceding the air puff location of the current training day). Because rats run more and faster laps when habituated to the air puff, a habituation index was calculated for each training session and animal as the total number of back-and-forth laps divided by the total time spent on the maze × 100. To obtain the air-puff-centered speed curves, the track positions were normalized and aligned to the air puff location for each session. In this plot (**Fig. 1c**), two sessions are missing due to corruption of the animal position data.

Firing rate (FR) changes between wakefulness and REM sleep were evaluated using the REM/wake ratios, calculated as (REM FR – wake FR)/(REM FR + wake FR). Positive ratios indicate REM FR > wake FR.

Ripple detection was performed by band-pass filtering (~100–200 Hz), squaring and normalizing, followed by thresholding of the field potential recorded in CA1 pyramidal layer. SPW-Rs were defined as events starting at 1 s.d., peaking at >4 s.d., and remaining at >1 s.d. for <130 ms and >20 ms around the peak. A control detection was performed on a nonhippocampal channel and all events simultaneously recorded from the hippocampal and control channels (for example, muscular noise) were removed. Ripple modulation was assessed using a Poisson test with $P < 0.001$. This approach tests whether the parameters for the Poisson cumulative distribution function of spikes outside SPW-Rs (baseline) are the same as for the Poisson cumulative function during SPW-Rs (custom program calling the "poiscdf" Matlab function). The baseline (inter-ripple) firing rate was computed during NREM sleep epochs excluding SPW-Rs. To avoid contamination of rate changes around SPW-Rs, the 100-ms periods before and after each ripple were also excluded.

Explained variance (EV) and reverse explained variance (REV) were calculated per session using subsets of cell pairs selected from the structures of interest. Only sessions with a minimum of 1 shank and 6 cells in each structure were included in the analysis. This criterion accounts for the variation in the number of sessions depending on the subset of cells the EV and REV are calculated for (pyramidal cell only vs. all cells). For REM sleep, only sessions with a minimum of 3 min of total REM sleep (all REM sleep epochs were pooled together) in both pre- and post-sleep were included. Pairwise correlations for EV and REV were calculated using the Pearson correlation coefficient on 50-ms-binned spike trains. The coefficients were separately calculated for pre-sleep (NREM or REM), training, and post-sleep (NREM or REM) periods and assembled into correlation matrices. The correlations between all combinations of these three matrices were then calculated and were used to assess the percentage of variance in the post-sleep period that could be explained by the patterns established during training while controlling for pre-existing correlations in the pre-sleep session (EV):

$$\mathrm{EV} = R^2_{T,S2\vee S1} = \left(\frac{R_{T,S2} - R_{T,S1} \times R_{S2,S1}}{\sqrt{\left(1 - R^2_{T,S1}\right)\left(1 - R^2_{S2,S1}\right)}} \right)^2$$

where *R* variables are the correlation coefficients between training (*T*), pre-sleep (*S*1) and post-sleep (*S*2) pairwise correlation matrices. The control value (REV) is obtained by switching the temporal order of the pre- and post-sleep session[17,18]. Only sessions with EV > REV for the first 20 min NREM epoch were used to calculate the decay of reactivations (EV/REV in first and subsequent 20-min NREM epochs; 6 sessions with EV > REV were excluded). Reactivations were considered significant when EV was significantly different from REV (Wilcoxon sign rank test). Comparisons of reactivation across time or structures were performed on the difference EV – REV (Wilcoxon rank sum tests).

doi:10.1038/nn.4637

An alternative approach was used to assess the contribution of individual cell pairs to replay. For this analysis, cell pairs were pooled (across sessions and animals) into 9 groups based on (i) the nature of hippocampal ripple-modulation of the BLA cell of the pair (up, down or none) and (ii) the significance of the Pearson correlation during training (positively correlated, negatively correlated ($P < 0.01$) or uncorrelated ($P > 0.01$) pairs). The nine groups and the number of pairs in each of these groups are summarized in **Supplementary Table 2**. Next, we computed (i) the difference between pre-NREM and post-NREM correlations for all pairs in each group, where the groups were compared by ANOVA followed by Bonferroni corrected multiple comparisons, and (ii) EV and REV for each subgroup, where the contribution of each pair was evaluated by calculating a global EV (all pairs) and then taking the difference between the global EV and recalculated EV without that pair (**Supplementary Fig. 10a**). A decrease in EV without that pair indicates a positive contribution of that pair. Since a single cell can participate in several pairs, a contribution per cell was also calculated by averaging the contributions of all pairs in which the cell participated. Cells and cell pairs were then pooled according to the magnitude of their contributions, using percentiles of the distribution of contributions (quartiles or 2.5th percentile of the left and right tails of the distribution). The gain in ripple upmodulation between pre- and post-NREM was calculated for each 10-ms bin by dividing the firing rate in each bin by the baseline firing rate outside SPW-Rs (inter-ripple NREM intervals). The mean peri-ripple gain was then calculated for each cell and averaged across cells. The data are shown for ±2-s windows for clarity. The statistics were performed on pre- and post-NREM ripple mean gains using a one-sided Wilcoxon signed rank test on the mean smoothed (20-ms Gaussian window) gain in a ±250-ms window centered at the ripple peak.

To calculate the reactivation strength R in pre-experience sleep and post-experience sleep epochs, BLA and hippocampal pyramidal cell spike trains were binned (50-ms bins) and z-scored. This gives Z_{bla} and Z_{hpc}, the $n_{Pyr} \times n_{Bins}$ z-scored spike count matrices for hippocampus and BLA. The hippocampus–BLA correlation matrix $C_{bla\text{-}hpc}$ for the training epoch (whole epoch or safe runs or air puff runs) was calculated as $C_{hpc-bla} = Z_{bla}Z_{hpc}{}^{T}/n_{Bins}$. The similarity between the training correlation matrix (whole run, safe or air puff trajectories) and the correlations at each time point of the pre-sleep and post-sleep epochs (reactivation strength R) was then calculated as $R(t) = z_{bla}(t)C_{bla-hpc}z_{hpc}(t)^{T}$, where $z_{bla}(t)$ and $z_{hpc}(t)$ are the population firing rate vectors of BLA and hippocampus neurons for the time bin t of either pre-experience sleep and post-experience sleep epoch. The reactivation strength R over time was then z-scored over the whole pre-NREM or post-NREM epochs. The peri-ripple reactivation strength was calculated for SPW-Rs occurring during pre-NREM and SPW-Rs occurring during post-NREM as the average R in a ±2-s window around ripple peaks (**Supplementary Fig. 10**) Finally, the mean peri-ripple reactivation strength R was computed over all rats and sessions. The significance of the difference in R between pre-experience NREM and post-experience NREM SPW-Rs was calculated on the mean R in a 500-ms window centered on the ripple peak using a Wilcoxon signed rank test. These methods used for evaluation of the reactivation strength were previously described for the reactivation of individual components following an ICA or PCA on the correlation matrix[26,53,54]. Because we were specifically interested in cross-structure reactivations and these previously used methods could not be directly applied, we used the raw correlation matrix instead of individual or principal components of the training correlation matrix to calculate reactivations strength.

Histology. At the end of experiments, small electrolytic lesions were made to mark the final position of the probes. Rats were euthanized with pentobarbital and perfused using saline and then 10% paraformaldehyde. The brains were extracted, sliced (70 µm), DAPI-stained and coverslipped. The sequential positions of the electrodes were reconstructed for all shanks from adjacent slices using the final position of the probe and the expected depth of the probe location for each recording day. This allowed the construction of histology maps showing the putative recorded location for each shank and each recording day (**Fig. 1f** and **Supplementary Fig. 2**). These maps were then used to restrict the analyses to specific amygdala nuclei.

Data availability. The data that support the main findings of this study will be publicly available on the CRCNS server (http://crcns.org/).

Code availability. All custom code is freely available on the Buzsáki Laboratory Github (https://github.com/buzsakilab/papers/tree/master/GGirardeau-BLAHpcInteractions-Package).

51. Vandecasteele, M. *et al.* Large-scale recording of neurons by movable silicon probes in behaving rodents. *J. Vis. Exp.* **3568**, e3568 (2012).
52. Hazan, L., Zugaro, M. & Buzsáki, G. Klusters, NeuroScope, NDManager: a free software suite for neurophysiological data processing and visualization. *J. Neurosci. Methods* **155**, 207–216 (2006).
53. Peyrache, A., Khamassi, M., Benchenane, K., Wiener, S.I. & Battaglia, F.P. Replay of rule-learning related neural patterns in the prefrontal cortex during sleep. *Nat. Neurosci.* **12**, 919–926 (2009).
54. Lopes-dos-Santos, V., Ribeiro, S. & Tort, A.B.L. Detecting cell assemblies in large neuronal populations. *J. Neurosci. Methods* **220**, 149–166 (2013).

nature research

Corresponding author(s): György Buzsáki

☐ Initial submission ☐ Revised version ☒ Final submission

Life Sciences Reporting Summary

Nature Research wishes to improve the reproducibility of the work that we publish. This form is intended for publication with all accepted life science papers and provides structure for consistency and transparency in reporting. Every life science submission will use this form; some list items might not apply to an individual manuscript, but all fields must be completed for clarity.

For further information on the points included in this form, see Reporting Life Sciences Research. For further information on Nature Research policies, including our data availability policy, see Authors & Referees and the Editorial Policy Checklist.

Experimental design

1. Sample size

Describe how sample size was determined.

No statistical method was used to pre-determine sample sizes but our sample sizes are similar to those typically reported in the field.

2. Data exclusions

Describe any data exclusions.

No data was systematically excluded. Data inclusion is reported in details in the methods section.

3. Replication

Describe whether the experimental findings were reliably reproduced.

N/A

4. Randomization

Describe how samples/organisms/participants were allocated into experimental groups.

N/A

5. Blinding

Describe whether the investigators were blinded to group allocation during data collection and/or analysis.

Experiments and analyses were not performed blind to the conditions of the experiments.

Note: all studies involving animals and/or human research participants must disclose whether blinding and randomization were used.

6. Statistical parameters

For all figures and tables that use statistical methods, confirm that the following items are present in relevant figure legends (or in the Methods section if additional space is needed).

n/a	Confirmed	
☐	☒	The exact sample size (*n*) for each experimental group/condition, given as a discrete number and unit of measurement (animals, litters, cultures, etc.)
☒	☐	A description of how samples were collected, noting whether measurements were taken from distinct samples or whether the same sample was measured repeatedly
☒	☐	A statement indicating how many times each experiment was replicated
☐	☒	The statistical test(s) used and whether they are one- or two-sided (note: only common tests should be described solely by name; more complex techniques should be described in the Methods section)
☐	☒	A description of any assumptions or corrections, such as an adjustment for multiple comparisons
☐	☒	The test results (e.g. *P* values) given as exact values whenever possible and with confidence intervals noted
☐	☒	A clear description of statistics including central tendency (e.g. median, mean) and variation (e.g. standard deviation, interquartile range)
☐	☒	Clearly defined error bars

See the web collection on statistics for biologists for further resources and guidance.

Nature Neuroscience: doi:10.1038/nn.4637

Software

Policy information about availability of computer code

7. Software

Describe the software used to analyze the data in this study.	Analyses were performed using Matlab and a combination of FMAToolbox (http://fmatoolbox.sourceforge.net/) and custom codes (https://github.com/buzsakilab/papers/tree/master/GGirardeau-BLAHpcInteractions-Package) .

For manuscripts utilizing custom algorithms or software that are central to the paper but not yet described in the published literature, software must be made available to editors and reviewers upon request. We strongly encourage code deposition in a community repository (e.g. GitHub). *Nature Methods* guidance for providing algorithms and software for publication provides further information on this topic.

Materials and reagents

Policy information about availability of materials

8. Materials availability

Indicate whether there are restrictions on availability of unique materials or if these materials are only available for distribution by a for-profit company.	N/A

9. Antibodies

Describe the antibodies used and how they were validated for use in the system under study (i.e. assay and species).	N/A

10. Eukaryotic cell lines

a. State the source of each eukaryotic cell line used.	N/A
b. Describe the method of cell line authentication used.	N/A
c. Report whether the cell lines were tested for mycoplasma contamination.	N/A
d. If any of the cell lines used are listed in the database of commonly misidentified cell lines maintained by ICLAC, provide a scientific rationale for their use.	N/A

Animals and human research participants

Policy information about studies involving animals; when reporting animal research, follow the ARRIVE guidelines

11. Description of research animals

Provide details on animals and/or animal-derived materials used in the study.	Long-Evans male rats, 3 months/300g at the time of experiments were used.

Policy information about studies involving human research participants

12. Description of human research participants

Describe the covariate-relevant population characteristics of the human research participants.	N/A

Nature Neuroscience: doi:10.1038/nn.4637